Periodicals of Engineering and Natural Sciences ISSN 2303-4521
Vol. 9, No. 2, April 2021, pp.830-841

Deformation and stress analysis of a U-shaped pipe compensator using a 3D scanner

Elvedin Kljuno[1], Faruk Razić[1], Alan Ćatović[1], Elmedin Mešić[1]
[1] Mechanical Engineering Faculty, University of Sarajevo

ABSTRACT

The paper shows a comparison of the three different methods to determine stress and strain in a U-shaped pipe compensator which is used to decrease stress in long pipes due to the constrained temperature dilatations. The stress and strain are analyzed analytically first with some parts of the analytical solution obtained numerically, such as integrals with no analytical solution in a closed form, i.e., functional series can be involved as a tool to solve those integrals.

The pipe is analyzed as a beam or a planar frame using the Castigliano's method to determine displacements. Since there are curved parts of the U compensator, the curved beam theory is applied. The alternative method to determine the strains and stresses along the pipe is shown using the numerical simulations in SolidWorks. The results are compared with the analytical solution. Finally, the experimental method using a 3D scanner is involved for a comparison to check the applied conditions in the analytical and the simulation model.

Keywords: U pipe compensator, Castigliano's method, deformation, normal stress, surface strain, strain measurement, 3D scanner

Corresponding Author:

Elvedin Kljuno

Mechanical Engineering Faculty, University of Sarajevo
Vilsonovo setaliste 9, 71000 Sarajevo, Bosnia
E-mail: kljuno@mef.unsa.ba

1. Introduction

If the dilatation of a long pipe is constrained in the direction of the pipeline, then the temperature change can cause structural integrity problems due to the significant stress which can easily pass over the yield strength of the material, even cause the pipeline destruction [1]. For this reason, an entire pipe segment is usually added [1] in the pipeline as shown in Fig. 1. The main purpose of introducing this segment of the pipeline is to allow that two ends of the compensator can slide inside or outside the compensator in the direction of the pipeline as much as the connected pipelines dictate due to the temperature change. The longer the connected pipeline the larger temperature dilatations have to be taken by the compensator ends. The compensator turns this longitudinal dilatation into bending along the U-shaped frame.

Figure 1. A thermal dilatation compensator in a pipeline [2]

Without compensator extremely large axial forces can occur since the pipeline cannot even buckle due to the constrained lateral displacement by the soil, wall, etc., depending on where the pipe is installed. Several other sources of stress in the pipeline wall are analyzed in [3] and [4]. The thermal stresses combined with other loadings [3,4] can cause plastic deformation of the pipeline.
Since the compensator contains several segments that can be considered straight line beams and curved beams, as shown in Fig. 2, the analytical determination of dilatations is consisted mainly of applied Castigliano's method [5, 6, 7] with specific cross-section of beams, which is the cross-section of a pipeline.

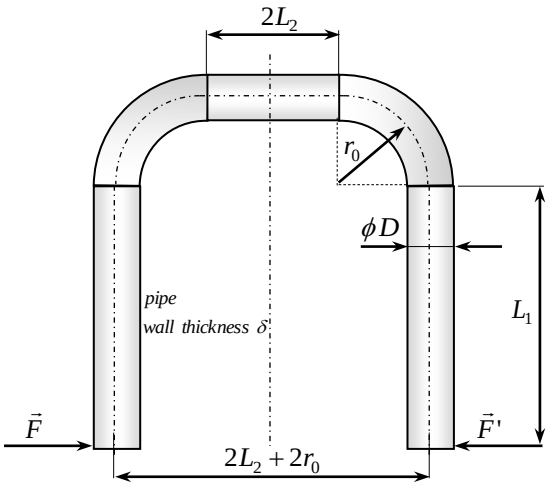

Figure 2. The U-shaped compensator segments

Alternatively, the method of elastic lines can be used as well [7] to establish the relationship between the force at the end of the compensator and the dilatation in the direction of the pipeline, i.e., in the direction of the force *F* in Fig. 2.

On the other hand, the U compensator can be modeled and simulated using numerical methods such as the finite element method [8] or the finite volume method [4, 9, 10]. The numerical method can be implemented in commercial software or some individually developed program packages, as explained in [4], to determine the corresponding dilatation for a given force in the direction of the pipeline. However, all that is mentioned above is related to modeling and can introduce errors through various assumptions of modeling process. Therefore, yet the third method is involved to determine what the real deformation is on the U-shaped compensator, and that is the 3D scanning that can determine the surface strain and displacements of the compensator surface points. In this way, both previous results can be compared with the experimental data.

For this purpose, ATOS Core 200 (GOM, GmbH) 3D scanner is used. The system records images of the loaded object, with specially prepared surface. The prepared surface contains black dots randomly applied, over a white (nonreflective) surface area of the U compensator, by spraying a part of the surface that is going to be analyzed. By monitoring the relative motion of the applied black points, the system calculates true or technical strain components with respect to the defined coordinate system (for more detailed explanation, see [11] and [12]).

2. Analytical method results

The compensator is consisted of several pipes that can be considered as beams, with the straight elastic line and the curved beams with elastic line in the shape of an arc, as shown in Fig. 3. To determine the deformation and the stiffness of the U compensator, several analytical methods can be used, such as Castigliano's method, elastic

line method, and variations of the methods based on elastic deformation energy [5, 6, 7]. The coordinate along the elastic line is the integration variable to solve for the energy of the elastic deformation, as shown in Fig. 3. The real loading of the U compensator at the end is by the force and the bending moment, since the pipe is connected in a way that it opposes the relative rotation of the cross-section, as well. However, since the stiffness with respect to the rotation at the end is relatively low, due to the assumption that a long pipe is connected to the compensator, here we consider that only a force is transferred from the pipe to the compensator.

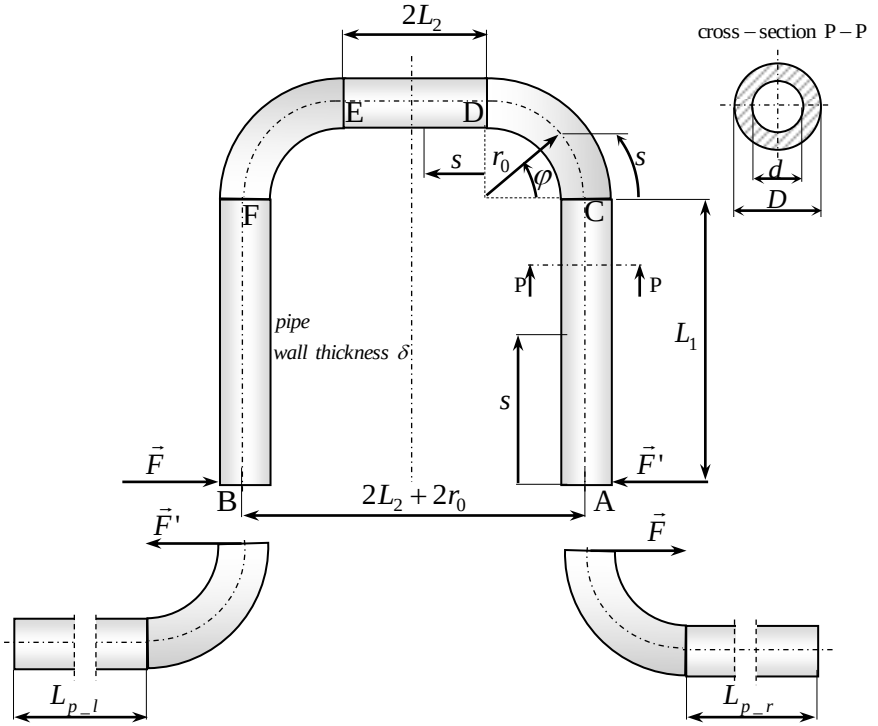

Figure 3. U compensator modeling (Horizontal plane)

Using the Castigliano's method [5, 6, 7], without neglecting any contribution of the axial and transversal forces in the deformation energy, first step in the analysis is to define the total deformation energy, as [7]

$$W_d = 2\left[\int_0^{L_1}\frac{M_x^2(s)}{2EI_x}ds + k_{t_1}\int_0^{L_1}\frac{F_t^2(s)}{2GA}ds + \int_0^{\frac{\pi}{2}}\frac{M_x^2(\varphi)}{2ES_n}d\varphi + \int_0^{\frac{\pi}{2}}\frac{F_n^2(\varphi)}{2EA}\underbrace{r_0 d\varphi}_{ds} + \right.$$

$$\left. + k_{t_\varphi}\int_0^{\frac{\pi}{2}}\frac{F_t^2(\varphi)}{2GA}ds + \int_0^{\frac{\pi}{2}}\frac{M_x\,(\varphi)F_n(\varphi)}{EA}d\varphi + \int_0^{L_2}\frac{M_x^2(s)}{2EI_x}ds + \int_0^{L_2}\frac{F_n^2(s)}{2EA}ds\right], \qquad (1)$$

where $S_n = eA$ is the static moment of inertia, e is the distance between neutral layer defined by the radius r_n and the center of the cross-section denoted by r_0, $e = r_0 - r_n$, F_t is the transversal force, F_n is the normal force to the considered cross-section, M_x is the bending moment, I_x is the moment of inertia, $I_x = \frac{(D^4-d^4)\pi}{64}$, E is the Young's modulus, $G = \frac{E}{2(1+\nu)}$ is the shear modulus and ν is the Poisson's ratio.

The radius of the neutral layer (where the normal stress due to the bending moment is equal zero) is calculated in the way that the total integral over the cross-section of the normal stress due to the bending moment is equal zero [5, 6, 7]:

$$r_n = \int_A \frac{dA}{r}, \qquad (2)$$

over the cross-section area A.

Factors k_{t_1} and k_{t_φ} are the scalars obtained via integrating the shear stress over the cross-section within the segment AC and the curved segment CD, respectively. Since the cross-section is the same, then the two factors are same $k_{t_1} = k_{t_\varphi} = k_t$.

Using the Castigliano's theorem, the displacement of one end with respect to the other end of the compensator is:

$$\frac{\partial W_d}{\partial F} = \delta_A = 2\left[\int_0^{L_1} \frac{M_x\,(s)}{EI_x}\frac{\partial M_x(s)}{\partial F}\;ds + k_t\int_0^{L_1}\frac{F_t\;(s)}{GA}\frac{\partial F_t(s)}{\partial F}ds + \int_0^{\frac{\pi}{2}}\frac{M_x\;(\varphi)}{ES_n}\;\frac{\partial M_x(\varphi)}{\partial F}d\varphi\right.$$

$$+\int_0^{\frac{\pi}{2}}\frac{F_n\;(\varphi)}{EA}\frac{\partial F_n}{\partial F}\;\underbrace{r_0 d\varphi}_{ds} + k_t\int_0^{\frac{\pi}{2}}\frac{F_t\;(\varphi)}{GA}\frac{\partial F_t}{\partial F}ds + \int_0^{\frac{\pi}{2}}\frac{\partial M_x\;(\varphi)}{\partial F}\;\frac{F_n(\varphi)}{EA}d\varphi +$$

$$\left.+\int_0^{\frac{\pi}{2}}\frac{M_x(\varphi)}{EA}\;\frac{\partial F_n\;(\varphi)}{\partial F}\;d\varphi + \int_0^{L_2}\frac{M_x\;(s)}{EI_x}\frac{\partial M_x(s)}{\partial F}\;ds + \int_0^{L_2}\frac{F_n\;(s)}{EA}\frac{\partial F_n\;(s)}{\partial F}ds\right], \tag{3}$$

Further, for the simplicity, the index in the bending moment will be omitted. The bending moment, the axial and the transversal force can be calculated over the three segment, up to the symmetry plane, as the following.

For the segment AC:

$$M = -Fs, \frac{\partial M}{\partial F} = -s, F_n = 0, F_t = F, \frac{\partial F_t}{\partial F} = 1,\ 0 \le s \le L_1. \tag{4}$$

For the curved segment CD:

$$M = -F(L_1 + r_0\sin\varphi), \frac{\partial M}{\partial F} = -(L_1 + r_0 sin\varphi), F_n = -Fsin\varphi, \frac{\partial F_n}{\partial F} = -sin\varphi,$$
$$F_t = Fcos\varphi, \frac{\partial F_t}{\partial F} = cos\varphi,\ 0 \le \varphi \le \frac{\pi}{2}. \tag{5}$$

For the segment DE:

$$M = -F(L_1 + r_0), \frac{\partial M}{\partial F} = -(L_1 + r_0), F_n = -F, \frac{\partial F_n}{\partial F} = -1, F_t = 0, 0 \le s \le L_2. \tag{6}$$

After the substitution of (4) to (6) into (3), the following is obtained:

$$\delta_A = 2\left[\frac{FL_1^3}{3EI_x} + \frac{k_t F L_1}{GA} + \frac{F}{E\,S_n}\left(L_1^2\varphi + 2L_1 r_0(-cos\varphi) + r_0^2 K(\varphi)\right)\Big|_0^{\frac{\pi}{2}} +\right.$$

$$+\frac{F}{EA}r_0 K(\varphi)\Big|_0^{\frac{\pi}{2}} + \frac{k_t r_0}{GA}F\left(\frac{\varphi}{2} + \frac{\sin(2\varphi)}{4}\right)\Big|_0^{\frac{\pi}{2}} + \frac{2F}{EA}(L_1(-cos\varphi) + r_0 K(\varphi))\Big|_0^{\frac{\pi}{2}} +$$

$$\left.\frac{F}{EI_x}(L_1 + r_0)^2 L_2 + \frac{F}{EA}L_2\right], \tag{7}$$

where $K(\varphi) = \frac{\varphi}{2} - \frac{\sin(2\varphi)}{4}$.

$$\delta_A = \frac{2FL_1}{EA}\left[\frac{AL_1^2}{3I_x} + 2k_t(1+\nu) + \frac{1}{e}\left(\frac{L_1\pi}{2} + 2r_0 + \frac{r_0^2}{L_1}\frac{\pi}{4}\right) +\right.$$

$$\frac{r_0}{L_1}\frac{\pi}{4}+\frac{k_t r_0}{\frac{L_1}{2(1+\nu)}}\frac{\pi}{4}+2\left(1+\frac{r_0}{L_1}\frac{\pi}{4}\right)+(L_1+r_0)^2\frac{A}{I_x}\frac{L_2}{L_1}+\frac{L_2}{L_1}\Bigg]. \quad (8)$$

The radius of the neutral layer, according to (2), considering the symmetry, is:

$$r_n = 2\int_{-\frac{\pi}{2}}^{\frac{\pi}{2}} d\theta \int_{\rho_1}^{\rho_2} \frac{\rho d\rho}{r_0+\rho\sin\theta} = 2\int_{-\frac{\pi}{2}}^{\frac{\pi}{2}} I_\rho d\theta \ . \quad (9)$$

The inner integral is:

$$I_\rho(\theta) = \int_{\rho_1}^{\rho_2} \frac{\rho d\rho}{r_0+\rho sin\theta} = \frac{\rho}{\sin\theta} - \frac{r_0}{\sin^2\theta}\ln(r_0+\rho\sin\theta)\Big|_{\rho_1}^{\rho_2} = \frac{\delta}{sin\theta} - \frac{r_0}{\sin^2\theta}\ln\left(\frac{r_0+\rho_2\sin\theta}{r_0+\rho_1 sin\theta}\right), \quad (10)$$

where, δ is the thickness of the pipe wall. The coordinates in (9) are shown in Fig. 4.

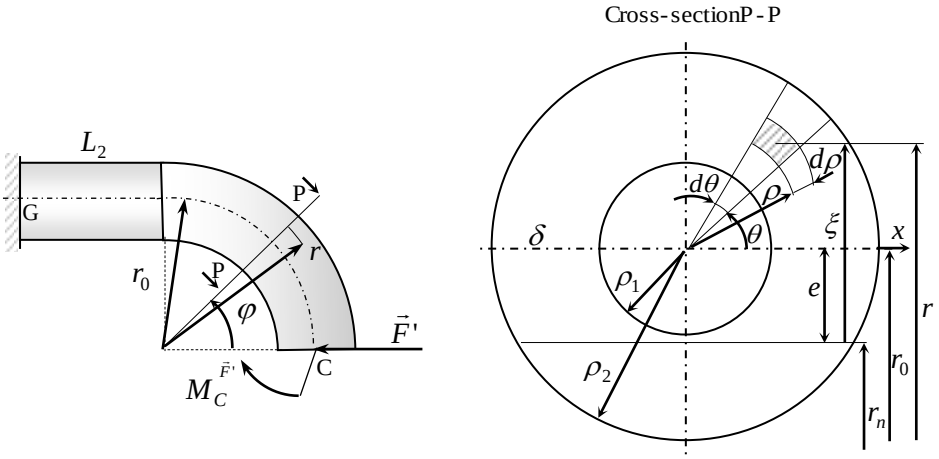

Figure 4. The cross-section and neutral layer position

Since there is a symmetry plane through G, then this cross-section has no rotation, and we can consider that the cross-section G is clamped. The moment $M_C^{\vec{F}'} = FL_1$.

The integral on the right hand-side of (9) can be calculated numerically using Matlab (or via functional series), as:

$$r_n = 0.5028\, r_0, \quad (11)$$

and

$$e = r_0 - r_n = 0.4972\, r_0. \quad (12)$$

The moment of inertia in (8) is:

$$I_x = \frac{(D^4-d^4)\pi}{64}, \quad (13)$$

where D and d are outer and inner diameter of the thick wall pipe. The cross-section area is:

$$A = \frac{(D^2-d^2)\pi}{4}. \quad (14)$$

The parameter k_t in general is defined as [5, 6, 7]:

$$k_t = A \int_A \frac{S_x'^2}{I_x^2 \eta^2(y)} dA, \tag{15}$$

where S_x' is the static moment of the part of the cross-section area from the distant side, below the line KT, with respect to the central axis x, $\eta(\xi)$ is the width of the material cross-section at the position y, as shown in Fig. 5.

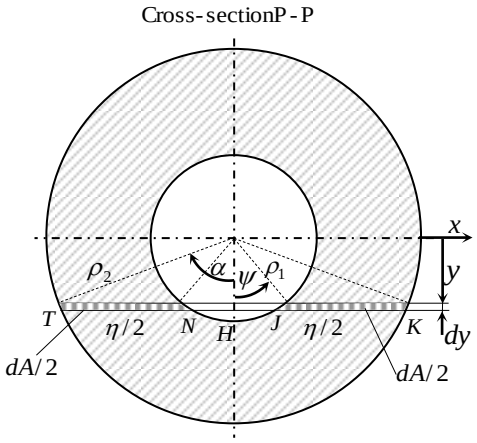

Figure 5. Calculation of the parameter k_t

In Fig. 5, the parameter η depends on *y* and geometrically is:

$$\eta(y) = \overline{JK}(y) + \overline{TN}(y) = 2\overline{JK}(y), \tag{16}$$

where the distance $\overline{JK}(y)$ is obtained as:

$$\overline{JK}(y) = \overline{HK}(y) - \overline{HJ}(y) = \rho_2 sin\alpha - \rho_1 sin\psi, \tag{17}$$

where ρ_1 and ρ_2 are the inner and outer radius of the thick-wall pipe, and the two angles are related from the geometry as:

$$\rho_2 cos\alpha = \rho_1 cos\psi = y. \tag{18}$$

From (18),

$$cos\alpha = \frac{y}{\rho_2}, \; cos\psi = \frac{y}{\rho_1}. \tag{19}$$

Using (16), (17) and (19), η becomes:

$$\eta(y) = 2\sqrt{\rho_2^2 - y^2} - 2\sqrt{\rho_1^2 - y^2}, \text{ for } 0 \le y \le \rho_1, \tag{20}$$

$$\eta(y) = 2\sqrt{\rho_2^2 - y^2}, \text{ for } \rho_1 \le y \le \rho_2. \tag{21}$$

The static moment of one part of the cross-section area, below or above the line parallel to x axis (see Fig 5.), at the distance *y* from the central axis, is for $\rho_1 < y \le \rho_2$:

$$S_x' = \int_{A'} \xi dA = \int_y^{\rho_2} \xi(\eta(\xi) d\xi) = \int_y^{\rho_2} \xi(\eta(\xi) d\xi) = \int_y^{\rho_2} \xi \left(2\sqrt{\rho_2^2 - \xi^2}) d\xi\right),$$

$$S_x' = \int_{\rho_2^2-y^2}^{0} -\frac{1}{2} d\lambda \left(2\sqrt{\lambda}\right) = \int_0^{\rho_2^2-y^2} \lambda^{\frac{1}{2}} d\lambda = \frac{2}{3}\lambda^{\frac{3}{2}}\Big|_0^{\rho_2^2-y^2} = \frac{2}{3}\sqrt{(\rho_2^2-y^2)^3}\,, \tag{22}$$

and for $0 \le y \le \rho_1$:

$$S_x' = \int_y^{\rho_1} \xi(\eta(\xi)d\xi) + \int_{\rho_1}^{\rho_2} \xi(\eta(\xi)d\xi) = I_1 + I_2, \tag{23}$$

where I_1 and I_2 are:

$$I_1 = \int_y^{\rho_1} \xi\left(2\sqrt{\rho_2^2-\xi^2} - 2\sqrt{\rho_1^2-\xi^2})d\xi\right),\ I_2 = \int_{\rho_1}^{\rho_2} \xi\left(2\sqrt{\rho_2^2-\xi^2}\right)d\xi. \tag{24}$$

The solution is analog to (22):

$$S_x' = \frac{2}{3}\sqrt{(\rho_2^2-y^2)^3} - \frac{2}{3}\sqrt{(\rho_1^2-y^2)^3},\ 0 \le y \le \rho_1. \tag{25}$$

Due to the property that it can be added and subtracted, the static moment of the area can be obtained using standard formulae for portion of a cycle below the line at *y* and subtracting the hollow portion of the inner cycle below the line *y*, which yields the same result.

Using (25) and (15):

$$k_t = A\int_A \frac{{S_x'}^2}{I_x^2\eta^2(y)}dA = \frac{A}{I_x^2}\int_A \frac{{S_x'}^2}{\eta^2(y)}\eta(y)dy = \frac{A}{I_x^2}\int_A \frac{{S_x'}^2}{\eta(y)}dy, \tag{26}$$

$$k_t = \frac{2A}{I_x^2}\left[\int_0^{\rho_1} \frac{\frac{4}{9}\left[(\rho_2^2-y^2)^{\frac{3}{2}}-(\rho_1^2-y^2)^{\frac{3}{2}}\right]^2}{2\left((\rho_2^2-y^2)^{\frac{1}{2}}-(\rho_1^2-y^2)^{\frac{1}{2}}\right)}dy + \int_{\rho_1}^{\rho_2} \frac{\frac{4}{9}(\rho_2^2-y^2)^3}{2(\rho_2^2-y^2)^{\frac{1}{2}}}dy\right], \tag{27}$$

where $I_x = \frac{(\rho_2^4-\rho_1^4)\pi}{4}$ and $A = (\rho_2^2-\rho_1^2)\pi$.

The integral in (27) is solved using programming in Matlab, for $\rho_1 = \frac{d}{2} = \frac{45.3}{2} = 22.7$ mm and $\rho_2 = \frac{D}{2} = \frac{53.5}{2}$ mm $= 26.8$ mm:

$$k_t = 1.494. \tag{28}$$

Finally, using (8), (12), (13), (14) and (28):

$$\delta_A = 0.417 \text{ mm}\,, \tag{29}$$

for the force of 6 kN and the Young's modulus of 110 GPa.

Using the approximate method for the corresponding rectangular frame, without the arc part of the U compensator (considering that CD and EF parts are without arc, but rectangular shape), then $\delta_A = 0.743$ mm. Significant influence of the bending of the beam in this case is noticeable, due to the significant contribution of the length of bending part of the frame with respect to the rest of the frame.

Maximum and minimum stress at the critical points of the cross-section in the middle of the U compensator are:

$$\sigma_{ext,p} = \frac{F(L_1+r_0)}{I_x}\frac{D}{2} - \frac{F}{A} = 97.1 \text{ MPa} - 9.65\text{MPa} = 87.45\text{MPa}\,, \tag{30}$$

$$\sigma_{ext,n} = -\frac{F(L_1+r_0)}{I_x}\frac{D}{2} - \frac{F}{A} = -97.1\ \text{MPa} - 9.65\text{MPa} = -106.75\text{MPa}\,. \quad (31)$$

Corresponding extreme (positive and negative) normal strain values at the critical points of the cross section are [5, 6, 7]:

$$\epsilon_p = \frac{1}{E}\left[\sigma_{ext,p} - \nu(\sigma_x + \sigma_y)\right] = \frac{\sigma_{ext,p}}{E} = 0.795 \cdot 10^{-3}, \quad (32)$$

$$\epsilon_n = \frac{1}{E}\left[\sigma_{ext,n} - \nu(\sigma_x + \sigma_y)\right] = \frac{\sigma_{ext,n}}{E} = -0.971 \cdot 10^{-3}, \quad (33)$$

where the two normal stress components, in the two directions in the plane of the cross-section, are equal zero.

The simplified analysis has been done for the case when there is no arc of the knee part of the compensator, which resulted in significantly different value for the dilatation. This shows that there is significant influence of the bending at the knee part and the theory of bended beams has to be used, since the pipe diameter is not negligible with respect to the radius of the knee. The following sections will describe the numerical simulations results and the experimental part, with the results that will be used for comparison with the analytical results above.

3. Experimental results obtained via 3D scanner and numerical simulations using Solid Works

The U pipe loading was simulated using the SolidWorks, with the same parameters and dimensions considered in the analytical part. The geometry and the results of the normal stress in the direction of the loading force are shown in Fig. 6.

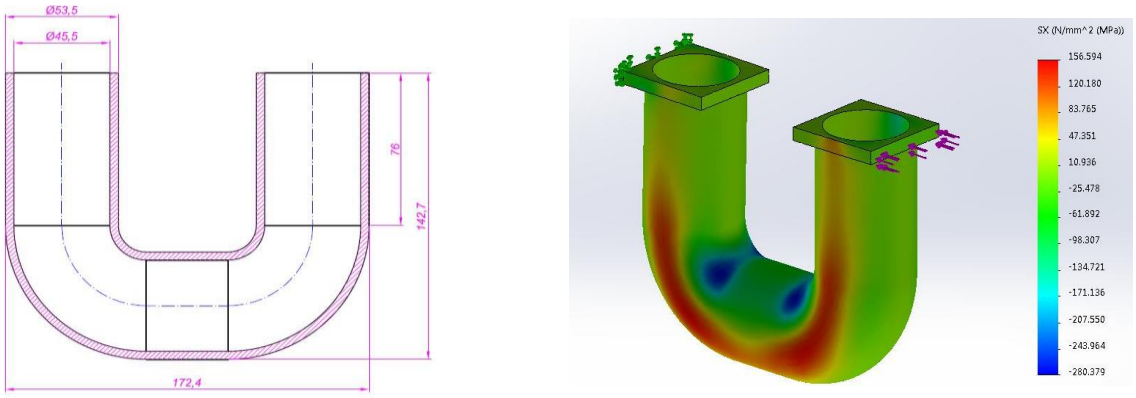

Figure 6. The geometry and the normal stress in the direction of the loading force obtained in Solid Works (the dimensions are given in millimeters)

The radius of the curvature of the central line is $r_0 = 40$ mm which is comparable with the outer and the inner diameter of the pipe, such that the analysis of the curved part of the frame cannot be analyzed using the theory of straight beams, which is one of the reasons that the analytical results deviate from the numerical analysis results for the curved part of the frame.

The experiment setup is shown in Fig.7, where a massive clamp was used and a force sensor that has the measurement range up to 150 kN. The clamp can generate force roughly up to 30 kN, using a wrench. For measuring the force, a precise voltmeter is used and an amplifier if relatively small values of force are used.

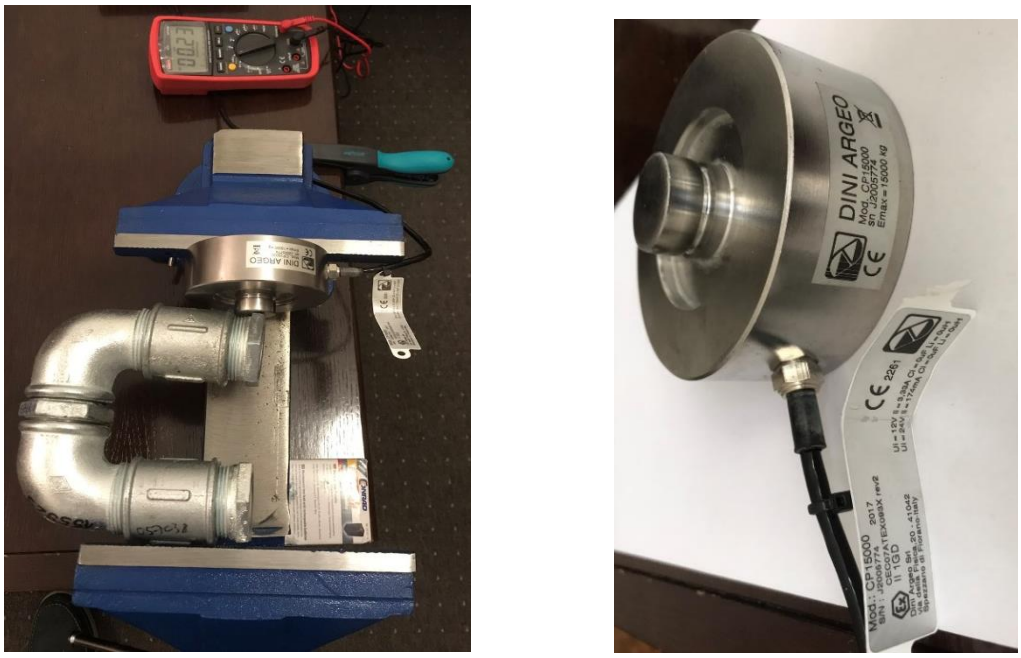

Figure 7. The loading of the U pipe using clamp (left) and the used force sensor (right)

To measure strain in on the 3D scanner, it is necessary to prepare the surface that is analyzed. The surface should not be reflective, such that the surface in Fig. 7 was sprayed with a non-reflective white color. Since the 3D scanner monitors the relative position of the a number of points at the surface, it is necessary to spray the surface of the U pipe with black non-reflective color, as shown in Fig. 8.

Figure 8. The surface preparation of the U pipe rough spray (left) and the fine spray (right)

Strain at the surface is detected by taking the reference image via scanner and several images during the deformation process, or a video. The change of the U pipe dimension in the direction of the loading can be measured by measuring the relative position of one side of the yaw with respect to the other, as shown in Fig. 9. Depending on the spray dots diameter, the scanner can register certain number of dots that can be used to measure relative position during the deformation of the knee part of the pipe, by applying the load using the clamp, as shown in Fig. 9.

The goal is to find an appropriate resolution and distribution of dots by spraying, such that the software registers a high number of dot pairs. The software GOM Correlate is installed on the laptop in Fig. 9 (left), which can automatically check for the preparedness of the object surface as shown in Fig. 9 (right). The diagram at right

hand-side shows the distribution in the green area, which shows that the spay was applied appropriately. This is the most difficult part of the measurement, since the spraying test is usually done several times until the appropriate distribution is reached, when the scanner software can register points on the surface.

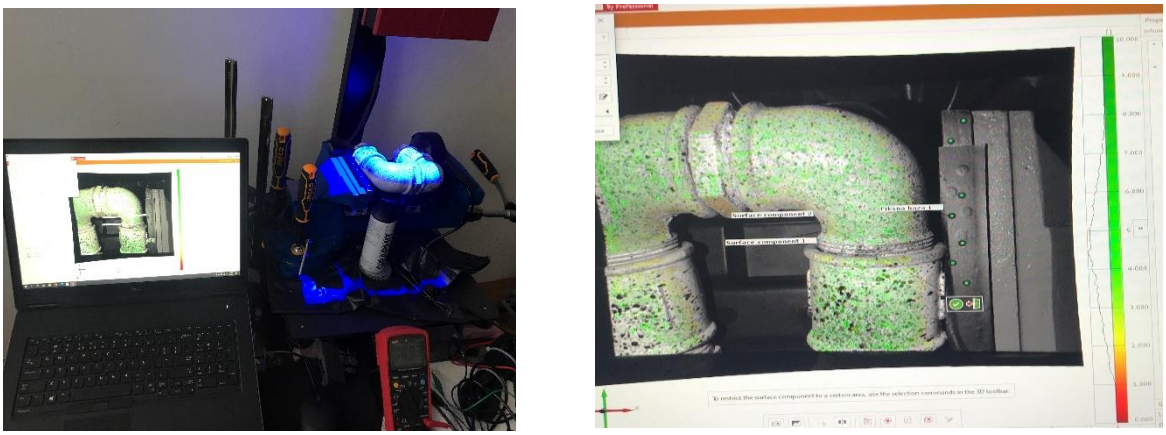

Figure 9. Taking images via scanner ATOS Core 200 (left) and registered points on the surface by the scanner (right)

If only one part of the surface is of an interest, such as the knee part of the U pipe, then the scanned and analyzed surface area can be redefined by the used, as shown in Fig. 10. The force of 6 kN was applied which caused the deformation that was registered by the scanner, as shown in Fig. 10. The motion of one part of the yaw can be registered relatively to the basis that is shown by the green dots to the right of the figure. The strain ϵ_x is the strain at the knee surface in the direction of the loading force, which is given in the percentage scale.

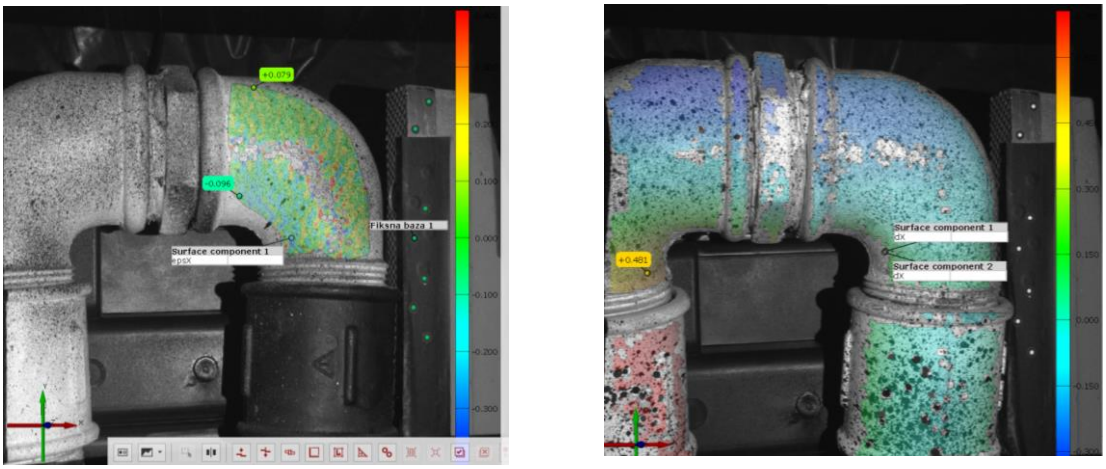

Figure 10. The results obtained using the 3D scanner for the strain (left) and for the displacement (right)

The influence of the gap in the threading was eliminated using the preloading on the clamp in such a way that the reference measurement started at the force of 600 N, rather than at zero force.

4. Results discussion

The only surface area that was considered is the knee, since the bending moment is about the maximum at this part of the U compensator, which means that deformations and surface strain are about the maximum in the absolute value.

Some of the differences between the analytical solution and the experiment are caused by the difference in the cross section of the straight parts. The knee part is also a bit different than the model in the analytical consideration. The real knee's cross-section gradually increases from one side to the other. The analytical model

uses the same cross-section all over the compensator, which is equal to the middle cross-section of the knee part.

By comparing the analytical method with the results obtained using the software and the results obtained using the 3D scanner, we can notice that there is relatively good agreement, although the software showed higher values for the normal stress in the direction of the loading force. However, the strain at the surface area is directly related to the stress via the Hooke's law, which provides the way to calculate the stress using the experimental results shown in Fig. 10 or we can calculate the strain analytically and compare it with the values in Fig. 10. Earlier, the strain values for the critical point are calculated analytically $\epsilon_p = 0.795 \cdot 10^{-3} = 0.0795 \cdot 10^{-2} = 0.0795\ \%$ and $\epsilon_n = -0.971 \cdot 10^{-3} = 0.0971 \cdot 10^{-2} = 0.0971\ \%$, which are relatively close to the values in Fig 9.

The values of the displacement have more significant deviation to the analytical solution, since there is significant movement of the clamp during the loading process, which causes errors in the filtering the rigid body motion part from the relative displacement of all registered points with respect to the basis (seven dots to the right of Fig. 10). The displacement δ_A represents the compensation of the thermal dilatations that depend on the temperature change of the connected pipes, their lengths, and the material property. This means that the displacement is the input data in the real application of the U compensator and from the analytical expression shown here, we can calculate the stress and strain of the U compensator.

5. Conclusion

The U compensator of thermal dilatations was analyzed using the theory of curved beams and the Castigliano's method. The deformation of the U pipe was directly corelated with the force caused by the thermal dilatations of connected long pipes. In the real applications, the displacement at the end of the U compensator is obtained as the total thermal dilatation of connected pipes and using the derived expressions, the generated force can be calculated. The analytical expressions were derived for the displacement, stress and strain at the critical points of the U compensator in order to compare them to the experimental values that were obtained using the 3D scanner.

Using a 3D scanner to experimentally determine the surface strain requires careful preparation of the surface. First, the surface has to be painted with white non-reflective color and then sprayed by black non-reflective color. The most difficult part of the scanning is to apply spray with the appropriate size of dots and appropriate density.

The comparison of the analytical results and the experimental results obtained using the 3D scanner showed no significant deviation, except the displacement value which had a certain amount of error due to the rigid body motion of the complete system with the clamp, such that the basis that was supposed to stay fixed was significantly moving during the loading process.

The future work can be focused on the direction of program development that would automatically determine the stress tensor components at any desired point inside the domain of the analyzed object based on the scanning of the object shape and based on the strain distribution across the surface area of the object.

Acknowledgment

Authors would like to thank to the colleague prof. dr. Muris Torlak for a discussion and his valuable inputs.

References

[1] M. Torlak, S. Metovic and E. Kljuno, Pipeline Systems for Transport and Distribution of Fluids: Hydraulic, Thermal and Mechanical Analysis, Mechanical Engineering Faculty Sarajevo, Sarajevo, 2020. (in Bosnian).

[2] "U-bends in underground district heating pipe made of plastic jacket composite pipe", 2009 (in German) [Online]. Available at: https://upload.wikimedia.org/wikipedia/commons/e/e8/Fernw%C3%A4rme_u_bogen.jpg (Accessed: 11 March, 2021.)

[3] E. Kljuno and M. Torlak, "Pipe Stress Analysis Using an Analytical and a Finite-Volume Method", In: Avdaković S., Volić I., Mujčić A., Uzunović T., Mujezinović A. (eds) *Advanced Technologies, Systems, and Applications V. IAT 2020. Lecture Notes in Networks and Systems*, vol 142. Springer, Cham., 2021, https://doi.org/10.1007/978-3-030-54765-3_35

[4] M. Torlak and E. Kljuno, "Analysis of Contact Mechanics Problems of Pipes Using a Finite-Volume Method", In: Avdaković S., Volić I., Mujčić A., Uzunović T., Mujezinović A. (eds) *Advanced Technologies, Systems, and Applications V. IAT 2020*. *Lecture Notes in Networks and Systems*, vol 142., Springer, Cham., 2021, https://doi.org/10.1007/978-3-030-54765-3_15

[5] S. Timoshenko and J.N. Goodier, Theory of elasticity, McGraw-Hill, New York, 1951.

[6] D. W. Rees, Mechanics of Solids and Structures, 2nd Edition, Imperial College Press, London, 2016.

[7] V. Dolecek, I. Karabegovic, D. Martinovic, M. Jurkovic, D. Blagojevic, S. Bogdan and I. Bijelonja, Elastostatika, University of Bihac, Bihac, 2004. (in Bosnian)

[8] R. Shih, Introduction to Finite Element Analysis Using SOLIDWORKS Simulation, 1st Edition, SDC Publications, Mission, 2020.

[9] I. Demirdzic and D. Martinovic, "Finite volume method for thermo-elasto-plastic stress analysis", *Computer methods in applied mechanics and engineering*, vol. 109, no. 3-4, pp. 331-349, 1993.

[10] I. Bijelonja, I. Demirdžić and S. Muzaferija, "A finite volume method for incompressible linear elasticity", *Computer methods in applied mechanics and engineering*, vol. 195, no. 44-47, pp. 6378-6390, 2006.

[11] E. Kljuno, F. Razic, E. Mesic and A. Catovic, "Structural stress and strain analysis using a 3D scanner", *Advanced Technologies, Systems, and Applications VI, IAT 2021,* Mostar, June 24-27, 2021, (in press).

[12] Y. Gao, T. Chengn, Y. Su, X. Xu, Y. Zhang and Q. Zhang, "High-efficiency and high-accuracy digital image correlation for three-dimensional measurement", *Optics and Lasers in Engineering*, vol. 65, pp. 73–80, 2015, http://dx.doi.org/10.1016/j.optlaseng.2014.05.013